

Remote epitaxy through graphene enables two-dimensional material-based layer transfer

Yunjo Kim^{1*}, Samuel S. Cruz^{1*}, Kyusang Lee^{1*}, Babatunde O. Alawode¹, Chanyeol Choi¹, Yi Song², Jared M. Johnson³, Christopher Heidelberger⁴, Wei Kong¹, Shinhyun Choi¹, Kuan Qiao¹, Ibraheem Almansouri^{1,5}, Eugene A. Fitzgerald⁴, Jing Kong^{2,6}, Alexie M. Kolpak¹, Jinwoo Hwang³ & Jeewan Kim^{1,4,6}

Epitaxy—the growth of a crystalline material on a substrate—is crucial for the semiconductor industry, but is often limited by the need for lattice matching between the two material systems. This strict requirement is relaxed for van der Waals epitaxy^{1–10}, in which epitaxy on layered or two-dimensional (2D) materials is mediated by weak van der Waals interactions, and which also allows facile layer release from 2D surfaces^{3,8}. It has been thought that 2D materials are the only seed layers for van der Waals epitaxy^{3–10}. However, the substrates below 2D materials may still interact with the layers grown during epitaxy (epilayers), as in the case of the so-called wetting transparency documented for graphene^{11–13}. Here we show that the weak van der Waals potential of graphene cannot completely screen the stronger potential field of many substrates, which enables epitaxial growth to occur despite its presence. We use density functional theory calculations to establish that adatoms will experience remote epitaxial registry with a substrate through a substrate–epilayer gap of up to nine ångströms; this gap can accommodate a monolayer of graphene. We confirm the predictions with homoepitaxial growth of GaAs(001) on GaAs(001) substrates through monolayer graphene, and show that the approach is also applicable to InP and GaP. The grown single-crystalline films are rapidly released from the graphene-coated substrate and perform as well as conventionally prepared films when incorporated in light-emitting devices. This technique enables any type of semiconductor film to be copied from underlying substrates through 2D materials, and then the resultant epilayer to be rapidly released and transferred to a substrate of interest. This process is particularly attractive in the context of non-silicon electronics and photonics, where the ability to re-use the graphene-coated substrates⁸ allows savings on the high cost of non-silicon substrates.

As a first step in investigating the role of the substrate below 2D materials on epitaxy, density functional theory (DFT) computations were performed to probe the transmission of crystallographic information of zinc-blende GaAs, a cubic crystal system, through graphene. A GaAs(001) substrate was chosen because of the crystallographic contrast between its cubic nature and hexagonal graphene, and the remote interaction between GaAs–GaAs (substrate–epilayer) was simulated using the plane-wave pseudopotential code as implemented in Quantum Espresso¹⁴. Planar averaged electron density was calculated as a function of the distance between GaAs substrates and GaAs epilayers (see Methods for detailed simulation procedure), with Fig. 1a, b illustrating the charge density between the As-terminated GaAs(001) substrate¹⁵ and a Ga- or As-initiated epitaxial layer separated by an empty space. Significant charge density is seen between the separated GaAs slabs, which disappears when the gap is increased beyond about 9 Å. This demonstrates an interaction between the slabs,

and suggests that remote epitaxy is possible within a 9-Å gap between substrate and epilayer. Calculated slab separation distances induced by inserting graphene in a GaAs–graphene–GaAs heterostructure suggest that the maximum number of graphene layers that can be inserted in the critical gap is two layers for As-terminated and Ga-initiated slabs, and one layer for As-terminated and As-initiated slabs (see Extended Data Fig. 1 for calculated natural separations for monolayer, bilayer and trilayer graphene). In practice, interaction between GaAs slabs may be damped by the vertical van der Waals force exerted by interlayer

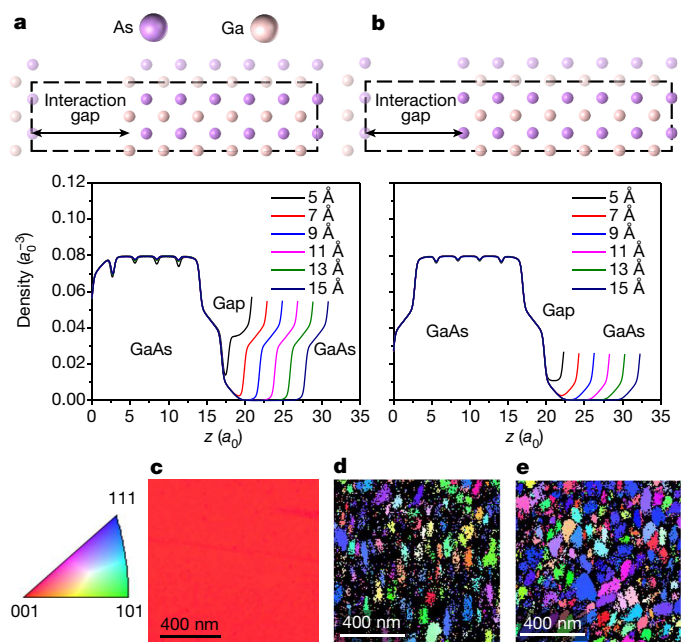


Figure 1 | Substrate–epilayer remote interaction with different gaps created by different numbers of stacked graphene interlayers.

a, b, Main plots, results of DFT calculations of averaged electron density along separated slabs of GaAs for As–Ga interaction (**a**) and As–As interaction (**b**). Periodic boundary conditions were imposed along the dashed lines of the simulation model (shown at top). Both plots show the existence of significant electron charge density between the separated slabs within a gap of about 9 Å. **c–e**, EBSD maps of GaAs grown on and exfoliated from ‘monolayer’ graphene–GaAs(001) substrate (**c**), showing (001) single-crystallinity, and of GaAs grown on and exfoliated from ‘bilayer’ (**d**) and ‘tetralayer’ (**e**) graphene–GaAs(001) substrate showing (111)-dominant polycrystallinity. On the left is the inverse pole figure colour triangle for crystallographic orientations.

¹Department of Mechanical Engineering, Massachusetts Institute of Technology, Cambridge, Massachusetts 02139, USA. ²Department of Electrical Engineering and Computer Science, Massachusetts Institute of Technology, Cambridge, Massachusetts 02139, USA. ³Department of Materials Science and Engineering, Ohio State University, Columbus, Ohio 43210, USA. ⁴Department of Materials Science and Engineering, Massachusetts Institute of Technology, Cambridge, Massachusetts 02139, USA. ⁵Department of Electrical Engineering and Computer Science, Masdar Institute of Science and Technology, Abu Dhabi 54224, United Arab Emirates. ⁶Research Laboratory of Electronics, Massachusetts Institute of Technology, Cambridge, Massachusetts 02139, USA. *These authors contributed equally to this work.

graphene, although it is about an order of magnitude weaker than that of covalent interactions. Thus, the true charge interaction gap between the substrate and epilayer through which crystallographic information can be transferred may be less than that estimated from the calculations.

To experimentally verify if remote homoepitaxy of GaAs through a graphene interlayer is possible, we prepared epitaxial templates by transferring monolayer, bilayer and tetralayer graphene onto GaAs(001) substrates. Native oxide on the GaAs substrates was etched away in HCl solution prior to immediate graphene transfer to ensure a pristine interface between graphene and GaAs. Next, epitaxial growth of GaAs films on the various graphene stacks on GaAs(001) substrates was performed (see Extended Data Fig. 2 for the topology of GaAs epilayer surfaces). To characterize the crystallographic orientation of the GaAs epilayer independently from that of the GaAs substrate, the GaAs epilayer was exfoliated from the graphene–GaAs substrate using a metal stessor⁸. Because the graphene interlayer completely separates the GaAs film from the GaAs substrate and allows precise release of GaAs films from the weakly attached graphene surface, the surface of the released side of GaAs presents a smooth finish after exfoliation⁸ (see Extended Data Fig. 2). This flat morphology enabled the use of electron backscatter diffraction (EBSD) mapping to identify domains of unique crystalline orientations in the GaAs epilayer. We found that the exfoliated GaAs epilayer grown on ‘monolayer’ graphene–GaAs(001) substrate exhibits (001) orientation, as indicated in red by the inverse pole figure (IPF) colour triangle (see Fig. 1c). This (001) orientation imprinted by the substrate disappears when GaAs films are grown on bilayer or tetralayer graphene (see Fig. 1d, e). X-ray diffraction using ω – 2θ scans of exfoliated GaAs epilayers also indicates that (001) single-crystallinity, present in GaAs grown on monolayer graphene, disappears for GaAs grown on bilayer and tetralayer graphene (see Extended Data Fig. 3). These observations indicate that remote epitaxy through the gap created by monolayer graphene is possible. Moreover, the large-scale view of an EBSD map of the exfoliated side of a GaAs film grown on graphene–GaAs(001) substrate in Fig. 2a shows (001) single-crystallinity. A high-resolution X-ray diffraction ϕ scan of the same exfoliated GaAs films (see Fig. 2b) shows four-fold symmetry of the diffraction peaks corresponding to GaAs(224) with

90° intervals, indicating that the GaAs grown on the GaAs(001) substrate through monolayer graphene is a single-crystalline zinc-blende phase without azimuthal rotations. Taken together, these observations confirm that the single-crystalline substrate is capable of transferring its epitaxial registry through a single graphene layer remotely to the epilayer, in good agreement with our critical gap calculation.

We note that merely placing monolayer graphene on the substrate does not guarantee perfect registry of the epilayer to the substrate. During the wet transfer of graphene grown on Cu foils via chemical vapour deposition, process-induced adsorbates can reside at the graphene surface and at transfer interfaces^{16,17} and need to be removed via annealing^{18–20} to enhance the proximity of graphene to the substrate (see Methods for the detailed annealing procedure). As shown in the EBSD map of GaAs grown on ‘un-annealed’ monolayer graphene transferred on a GaAs substrate, the resulting GaAs films are not epitaxial to the substrate (see Fig. 2c). To ensure a clean interface in the graphene transfer, we use a layer-resolved graphene transfer (LRGT) process²¹ whereby a metal stessor is used to exfoliate monolayer epitaxial graphene from a SiC substrate immediately followed by dry-transfer onto the GaAs substrate. The LRGT process ensures single-crystalline growth via remote epitaxy without the need for annealing. We find that regardless of the type of graphene and its alignment to the substrate, GaAs epilayers are registered to the GaAs substrate through monolayer graphene.

The remote epitaxial alignment between a GaAs(001) epilayer and a GaAs(001) substrate was atomically resolved by performing cross-sectional scanning transmission electron microscopy (STEM). Figure 2d shows STEM images at different magnifications which reveal that the GaAs(001) epilayer is epitaxially aligned with the GaAs(001) substrate through the gap created by monolayer graphene. The measured gap between the GaAs epilayer and the substrate is about 5 Å, which is below the critical gap calculated with DFT. In Fig. 2d, the monolayer graphene is visible between the epitaxial layer and the substrate (indicated by the arrow). Identical convergent beam electron diffraction patterns from the epilayer and the substrate also confirm the epitaxial relationship. We also investigated the dislocation density using low-angle annular dark field imaging of the GaAs–graphene–GaAs sample

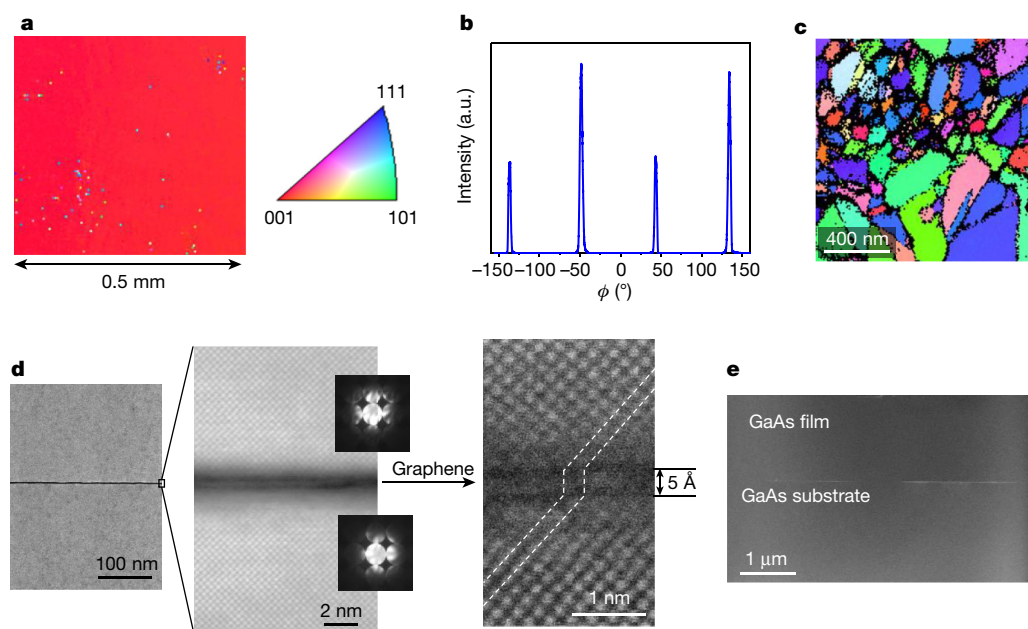


Figure 2 | Characterization of GaAs grown on the monolayer graphene–GaAs(001) substrate. **a**, Large-scale EBSD map of exfoliated GaAs. **b**, High-resolution X-ray diffraction azimuthal off-axis ϕ scan of the same exfoliated GaAs layer, representing a single-crystalline zinc-blende structure without in-plane rotations. **c**, EBSD map of an exfoliated GaAs layer grown on a monolayer graphene–GaAs substrate without H₂ annealing after transfer.

d, High-resolution STEM images showing excellent remote alignment of the GaAs(001) lattices through the graphene. Convergent-beam electron diffraction patterns from the epilayer (top inset) and the substrate (bottom inset) show identical zinc-blende (001) orientations. **e**, Low-angle annular dark field STEM image showing no dislocations.

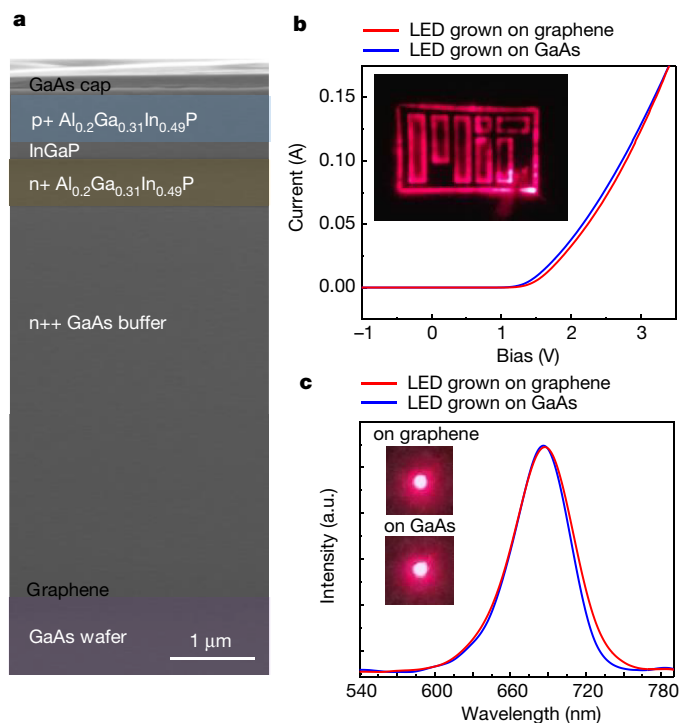


Figure 3 | AlGaInP-GaInP double heterojunction LEDs on a graphene-GaAs substrate. **a**, Cross-sectional SEM image of heterojunction LEDs. **b**, I - V curves of LEDs grown on graphene-GaAs substrates and directly on GaAs. Inset, emitted red light from the LEDs grown on the graphene-GaAs substrate. **c**, Electroluminescence spectra of the LEDs grown on graphene-GaAs substrates and directly on GaAs. Inset, photographs of functioning LEDs grown on both substrates.

at low magnification in cross-sectional STEM (see Fig. 2e); we found no evidence for strain contrast at the substrate-epilayer interface—which typically appears when dislocations are present—in these

images. This implies that no dislocations are present, at least not in the inspected area. Moreover, no anti-phase domains appeared to have nucleated at the graphene interface. Although the TEM inspection covered only a limited sample area, corresponding to the conventional size of TEM samples prepared by a focused ion beam, it does confirm that remote homoepitaxial growth of GaAs through flat graphene on GaAs substrates does occur.

Steady-state room-temperature photoluminescence spectra of exfoliated GaAs, grown on graphene-GaAs substrates, are comparable to spectra recorded for GaAs wafers (Extended Data Fig. 4), indicating no degradation in material quality during growth/transfer processes. This motivated us to grow AlGaInP-GaInP double heterojunction light-emitting diodes (LEDs) on graphene-GaAs substrates (see Fig. 3a for cross-sectional scanning electron microscopy of heterojunction LEDs). Such devices exhibited I - V curves and turn-on voltages of 1.3 V that are comparable to those of LEDs directly grown on a bare GaAs substrate (Fig. 3b, with the inset illustrating red light emission from LEDs grown through remote epitaxy). Electroluminescence spectra of the LEDs grown on GaAs, either through remote epitaxy with graphene or conventionally without graphene, confirmed their nearly identical performance, with very similar full-width at half-maxima of 45 ± 5 nm and peak electroluminescence intensities at an injection current of 250 mA (see Fig. 3c). The insets of Fig. 3c show photographs of functioning LEDs grown on GaAs with and without graphene. The LEDs were exfoliated and transferred to the Si substrate, which minimally degrades the LED performance as indicated by the comparable I - V curves and light emission before and after the transfer (see Extended Data Fig. 5).

To investigate if remote homoepitaxy can be applied to other general material systems, we have performed epitaxial growth of InP and GaP on InP(001) and GaP(001) substrates, respectively, with an overlayer of monolayer graphene. As shown in Fig. 4, single-crystalline GaAs(001), InP(001) and GaP(001) films were successfully grown via remote homoepitaxy and exfoliated. Characterizations based on high-resolution X-ray diffraction and EBSD measurements (shown in Fig. 4d-f and g-i, respectively) confirm the single-crystal nature of

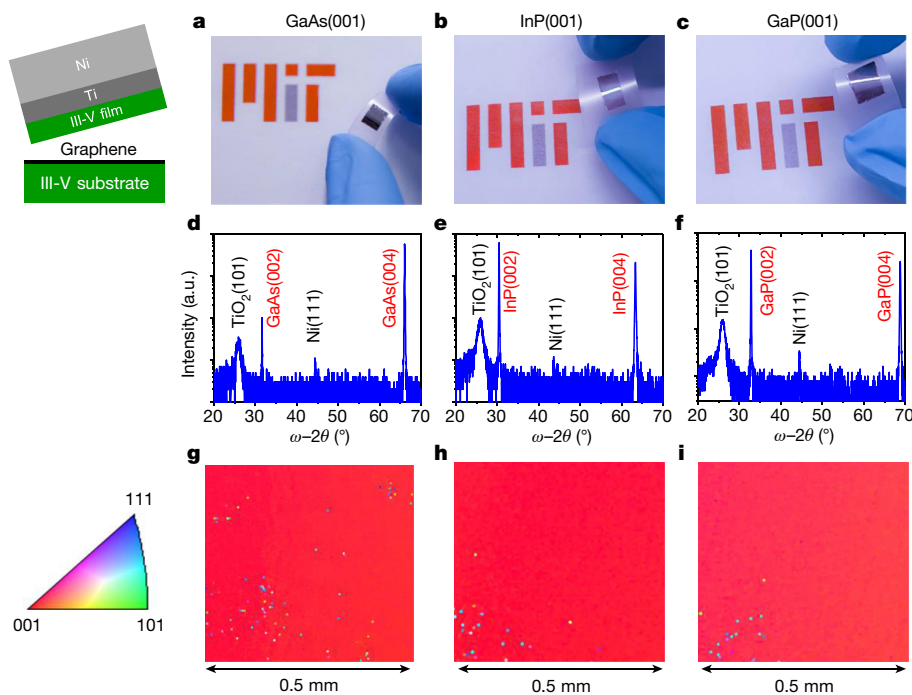


Figure 4 | Single-crystalline III-V(001) films exfoliated from graphene-III-V(001) substrates after remote epitaxy. **a**, **d**, **g**, GaAs; **b**, **e**, **h**, InP; **c**, **f**, **i**, GaP. Schematic illustration (top left) shows the exfoliation process of thin-film sample preparation for high-resolution X-ray diffraction and EBSD characterizations. **a**-**c**, Photographs of single-crystalline

GaAs(001), InP(001), and GaP(001) films exfoliated from graphene-III-V(001) substrates. **d**-**f**, High-resolution X-ray diffraction ω - 2θ scans of the exfoliated semiconductor/stressor stack that includes GaAs(001), InP(001), and GaP(001) epilayers. **g**-**i**, Large-scale EBSD maps of GaAs(001), InP(001), and GaP(001) epilayer surfaces.

GaAs, InP and GaP films grown by remote epitaxy that support the feasibility of our 2D material-based layer transfer (2DLT) technique for general material systems. In addition, the crystalline orientation can be manipulated by changing the orientation of the substrate. Single-crystalline GaAs(111) films have been grown on monolayer graphene–GaAs(111)B substrate as shown in Extended Data Fig. 6. Graphene is known to remain pristine during epitaxy without dissolving into substrates or epilayers owing to its high thermal stability^{8,22,23}, thus all epitaxial materials investigated in this study were successfully exfoliated by a Ti/Ni stressor^{8,24}, as shown in Fig. 4a–c. Epilayers failed to exfoliate when epitaxy was performed on a substrate with a graphene overlayer that had been pre-damaged by Ar plasma treatment. As shown in Extended Data Figs 2a and 7, the smooth morphology of the exfoliated epilayer surface⁸ suggests precise release from pristine graphene⁸. Note that rough spalling marks observed in very limited areas originated from direct epitaxy through localized defects/holes in the graphene which remains to be addressed by improving the yield of graphene transfer (see Extended Data Fig. 7). The ease of applying this 2DLT technique to a multitude of systems will allow less common semiconductors such as InP to see common use in various applications.

Our results indicate that remote homoepitaxy is possible due to the interaction between substrate and epilayer through monolayer graphene, which is sufficiently thin and electrically penetrable to guide the epitaxial orientation of overlayers. Since the epilayers grown by remote homoepitaxy can be released from the graphene surface, this 2DLT technique offers the potential to grow, transfer and stack any electronic and photonic materials on 2D materials without the lattice matching limitation. This will open a pathway towards defect-free heterointegration of dissimilar materials while saving the cost of expensive and exotic substrates.

Online Content Methods, along with any additional Extended Data display items and Source Data, are available in the online version of the paper; references unique to these sections appear only in the online paper.

Received 24 October 2016; accepted 3 March 2017.

1. Koma, A., Sunouchi, K. & Miyajima, T. Fabrication and characterization of heterostructures with subnanometer thickness. *Microelectron. Eng.* **2**, 129–136 (1984).
2. Ueno, K., Saiki, K., Shimada, T. & Koma, A. Epitaxial-growth of transition-metal dichalcogenides on cleaved faces of mica. *J. Vac. Sci. Technol. A* **8**, 68–72 (1990).
3. Chung, K., Lee, C. H. & Yi, G. C. Transferable GaN layers grown on ZnO-coated graphene layers for optoelectronic devices. *Science* **330**, 655–657 (2010).
4. Shi, Y. *et al.* van der Waals epitaxy of MoS₂ layers using graphene as growth templates. *Nano Lett.* **12**, 2784–2791 (2012).
5. Gehring, P., Gao, B. F., Burghard, M. & Kern, K. Growth of high-mobility Bi₂Te₂Se nanoplatelets on hBN sheets by van der Waals epitaxy. *Nano Lett.* **12**, 5137–5142 (2012).
6. Gupta, P. *et al.* MOVPE growth of semipolar III-nitride semiconductors on CVD graphene. *J. Cryst. Growth* **372**, 105–108 (2013).
7. Zhang, Y. *et al.* Direct observation of the transition from indirect to direct bandgap in atomically thin epitaxial MoSe₂. *Nat. Nanotechnol.* **9**, 111–115 (2013).
8. Kim, J. *et al.* Principle of direct van der Waals epitaxy of single-crystalline films on epitaxial graphene. *Nat. Commun.* **5**, 4836 (2014).

9. Lin, Y. C. *et al.* Direct synthesis of van der Waals solids. *ACS Nano* **8**, 3715–3723 (2014).
10. Alaskar, Y. *et al.* Theoretical and experimental study of highly textured GaAs on silicon using a graphene buffer layer. *J. Cryst. Growth* **425**, 268–273 (2015).
11. Shih, C. J., Strano, M. S. & Blankschtein, D. Wetting translucency of graphene. *Nat. Mater.* **12**, 866–869 (2013).
12. Rafiee, J. *et al.* Wetting transparency of graphene. *Nat. Mater.* **11**, 217–222 (2012).
13. Raj, R., Maroo, S. C. & Wang, E. N. Wettability of graphene. *Nano Lett.* **13**, 1509–1515 (2013).
14. Giannozzi, P. *et al.* QUANTUM ESPRESSO: a modular and open-source software project for quantum simulations of materials. *J. Phys. Condens. Matter* **21**, 395502 (2009).
15. Biegelsen, D. K., Bringans, R. D., Northrup, J. E. & Swartz, L. E. Surface reconstructions of GaAs(100) observed by scanning tunneling microscopy. *Phys. Rev. B* **41**, 5701–5706 (1990).
16. Temmen, M., Ochedowski, O., Schleberger, M., Reichling, M. & Bollmann, T. R. J. Hydration layers trapped between graphene and a hydrophilic substrate. *New J. Phys.* **16**, 053039 (2014).
17. Chhikara, M., Pavlica, E., Matkovic, A., Gajic, R. & Bratina, G. Effect of water layer at the SiO₂/graphene interface on pentacene morphology. *Langmuir* **30**, 11681–11688 (2014).
18. Cheng, Z. *et al.* Toward intrinsic graphene surfaces: a systematic study on thermal annealing and wet-chemical treatment of SiO₂-supported graphene devices. *Nano Lett.* **11**, 767–771 (2011).
19. Lin, Y. C. *et al.* Graphene annealing: how clean can it be? *Nano Lett.* **12**, 414–419 (2012).
20. Kumar, K., Kim, Y. S. & Yang, E. H. The influence of thermal annealing to remove polymeric residue on the electronic doping and morphological characteristics of graphene. *Carbon* **65**, 35–45 (2013).
21. Kim, J. *et al.* Layer-resolved graphene transfer via engineered strain layers. *Science* **342**, 833–836 (2013).
22. Kiraly, B. *et al.* Electronic and mechanical properties of graphene-germanium interfaces grown by chemical vapor deposition. *Nano Lett.* **15**, 7414–7420 (2015).
23. Cho, J. *et al.* Atomic-scale investigation of graphene grown on Cu foil and the effects of thermal annealing. *ACS Nano* **5**, 3607–3613 (2011).
24. Bedell, S. W. *et al.* Kerf-less removal of Si, Ge, and III-V layers by controlled spalling to enable low-cost PV technologies. *IEEE J. Photovolt.* **2**, 141–147 (2012).

Acknowledgements This work was partly supported by the One to One Joint Research Project of the MI/MIT Cooperative Program. We thank the LG Electronics R&D Center for partial support of the GaAs 2DLT programme. We also thank the LAM Research Foundation, Analog Devices, Inc. and the MIT Lincoln Laboratory for general support; and Y. S. Lee of IBM, D. Sadana of IBM, A. Yoon of LAM Research, R. J. Molnar of MIT Lincoln Laboratory, C. V. Thompson of MIT, and J. Lee of LG Electronics for discussions. J. Kim thanks M. Baldo, D. Ha, and K. Jung of MIT for their assistance with electroluminescence measurements. S.S.C. thanks the National Science Foundation for a graduate research fellowship (grant no. 1122374). Y. S. and J. Kong thank support for Y.S. from NSF (DMR/ECCS – 1509197). J. H and J.M.J thank support for J.M.J from NSF (MRSEC DMR-1420451).

Author Contributions J. Kim conceived the 2DLT process, designed experiments, and directed the team. Y.K., S.S.C., K.L., C.C., Y.S., C.H., W.K., S.C., K.Q. and I.A. performed the epitaxial growths/transfer experiments and characterization. K.L. fabricated and measured LED devices. J.M.J. and J.H. performed TEM analysis. B.O.A. contributed to the computational model and DFT simulation. All authors contributed to the discussion and analysis of the results regarding the manuscript.

Author Information Reprints and permissions information is available at www.nature.com/reprints. The authors declare no competing financial interests. Readers are welcome to comment on the online version of the paper. Publisher's note: Springer Nature remains neutral with regard to jurisdictional claims in published maps and institutional affiliations. Correspondence and requests for materials should be addressed to J.K. (jeehwan@mit.edu).

METHODS

Graphene formation and transfer. GaAs films were grown on CVD graphene or epitaxial graphene transferred on GaAs(001) wafers without precise alignment. CVD graphene was synthesized on a Cu foil using low pressure CVD. Cu foil was annealed in a quartz tube furnace at 1,000 °C for 30 min under 10 standard cubic centimetres per minute (sccm) of H₂ flow. Graphene growth proceeded under 4 sccm of CH₄ and 70 sccm of H₂ flow for 30 min at 1.90 torr. Graphene growth was terminated by a self-limiting process, yielding a monolayer of polycrystalline graphene. For the transfer process, poly(methyl-methacrylate) (PMMA) was spin-cast onto graphene coated Cu foil and baked at 80 °C for 10 min. Using the PMMA as a 'handle', the Cu foil was dissolved in FeCl₃ copper etchant solution for 15 min. While the graphene-PMMA stack was held on the water surface by surface tension, the stack was transferred onto a GaAs substrate after its oxide was removed by 10% hydrochloric acid solution. The substrate was dried at 80 °C for 10 min and then the PMMA 'handle' was dissolved in acetone. Annealing of transferred CVD graphene on GaAs substrates was performed at 350 °C for 30 min in ambient H₂ to remove the process residues at the interface and promote better adhesion. Epitaxial graphene was grown on a Si-face 4H-SiC(0001) wafer. Graphitization of SiC was performed at 1,575 °C for 1 h to form monolayer graphene in ambient Ar. The graphene was completely exfoliated using the LRGT process, in which a Ni stressor layer was deposited on epitaxial graphene and the graphene-Ni stack was removed from SiC using a thermally released tape handling layer. The graphene-Ni stack was immediately transferred to HCl-treated GaAs substrates followed by the removal of the thermal tape by annealing just above the release temperature of 90 °C. Then the Ni stressor layer was removed by dipping into acids.

Epitaxial growth. Epitaxial growth of GaAs was performed on CVD graphene transferred onto GaAs(001) substrates in a close coupled showerhead MOCVD reactor. For GaAs growth, arsine and trimethylgallium were used as the precursors for As and Ga sources. The growth was divided into two parts. First, the growth proceeded at a relatively low temperature of 450 °C at 100 torr for a short time to encourage the nucleation of GaAs islands on graphene to initiate the growth. The reactor temperature was then ramped to 650 °C for normal growth of GaAs. For GaP and InP growth, phosphine, trimethylgallium and trimethylindium were used as P, Ga and In sources, respectively, the growth conditions proceeded in the same manner as the GaAs growth in the MOCVD reactor. The LED device stack was regrown on a 4 μm thick n-GaAs buffer layer in the MOCVD reactor, with 800 nm of Si doped n-AlGaInP, 100 nm of GaInP, 800 nm of Zn doped p-AlGaInP and 100 nm of p-GaAs as a capping layer. The device was grown at 650 °C under N₂ flow as ambient carrier gas.

Computational model. As-termination of GaAs(001) slabs was selected for computational modelling as the growth conditions of the epitaxial layer imply an As pre-layer terminating the ends of the slabs. DFT computations were performed to determine the interaction of As- and Ga-terminated layers of GaAs(001) on the As-terminated substrate. The computations were done using the plane-wave pseudopotential code Quantum Espresso¹⁴. We found the convergence of the number

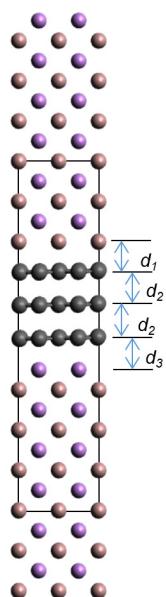
of layers of GaAs(001) slab to be 12. In all our calculations, all atoms (Ga, As) were relaxed. A *k*-point mesh of 4×4×1 was selected. For the local exchange correlation functional, the Perdew-Burke-Ernzerhof general gradient approximation was used²⁵. The spacing between periodic images of the superstructure in the *z* direction was varied between 5 Å and 30 Å. The in-plane lattice constant was fixed to 1×1 times the calculated lattice constant (5.63 Å) of bulk GaAs. An ideal case of a 1×1 system was modelled for the simulation as surface reconstructions do not significantly affect the behaviour of the surface at the interface^{26,27}. The relaxation calculations were set to complete when the forces on the relaxed layers were less than 1×10⁻³ a.u. We employed wavefunction and charge density kinetic energy cut-offs of 50 Ry and 350 Ry, respectively.

Exfoliation of GaAs from graphene surface. Deposition of a 100 nm Ti adhesion layer and a high stress Ni stressor layer on the GaAs epilayer surface induces strain at the GaAs-graphene interface. By applying the thermal-release handling tape, fast release of the GaAs epilayer occurs from the graphene surface.

Light-emitting diodes. After remote epitaxy, the front contact is patterned by photolithography using an LOR 3A and SPR 220 bilayer photoresist process. Then, a Pd(5 nm)/Ge(20 nm)/Au(100 nm) metal contact is deposited by e-beam evaporation. The 100 μm diameter contact pad is patterned at the centre of the device. After the metal layer is lifted off, 200 μm × 200 μm mesas are defined by photolithography using SPR 220 and chemical etching using HCl:H₃PO₄ (3:1) solution. The LEDs are annealed for 1 h at 200 °C for ohmic contact formation. For 2DLT processed LEDs, 50 nm of titanium is deposited by thermal evaporation on the as-grown sample then nickel was sputter deposited to a thickness of 6 μm with argon plasma. Thermal release tape is applied to the metal stressor/as-grown sample heterostructure, followed by pulling the thermal release tape from the substrate edge to obtain exfoliation from the graphene interface. For thin films transferred to silicon, polydimethylsiloxane (PDMS) was spin-coated onto a Si(001) wafer at 2,000 r.p.m. for 30 s, followed by baking in an oven at 80 °C for 2 min. The exfoliated film is then placed on the PDMS and pressure is applied. The thermal tape holding the film is then removed by heating the entire structure on a hot plate at 125 °C until the tape is thermally released. The bonded stack is left to cool at room temperature for 30 min. Nickel and titanium are removed by FeCl₃ solution (20% w/v) and dilute HF. After the film transfer, the same fabrication method is applied for the substrate-based LED described above. The LEDs are tested under continuous-wave (CW) conditions.

Data Availability. The data that support the findings of this study are available from the corresponding author upon reasonable request.

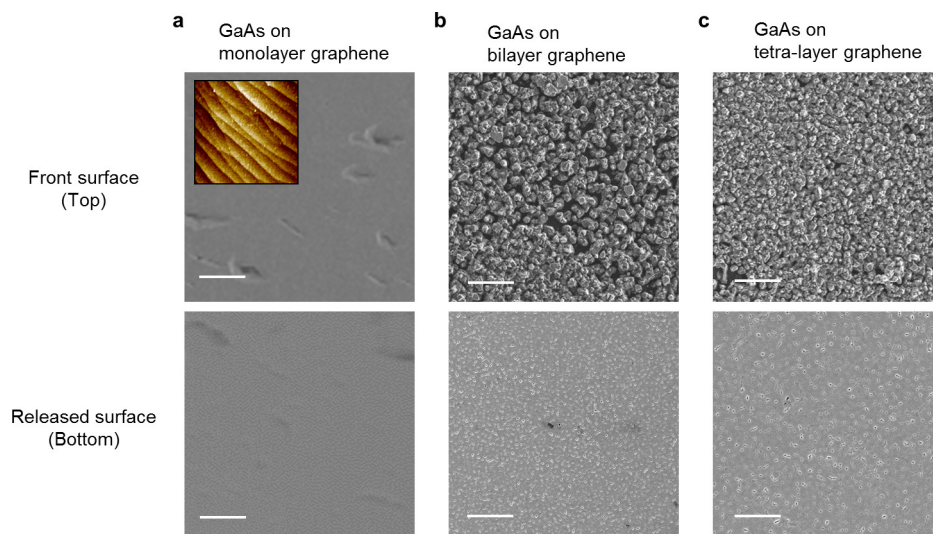
- Perdew, J. P., Burke, K. & Ernzerhof, M. Generalized gradient approximation made simple. *Phys. Rev. Lett.* **77**, 3865–3868 (1996).
- Kneedler, E. M. *et al.* Influence of substrate surface reconstruction on the growth and magnetic properties of Fe on GaAs(001). *Phys. Rev. B* **56**, 8163–8168 (1997).
- Moosbühler, R., Bensch, F., Dumm, M. & Bayreuther, G. Epitaxial Fe films on GaAs(001): does the substrate surface reconstruction affect the uniaxial magnetic anisotropy? *J. Appl. Phys.* **91**, 8757–8759 (2002).



Terminations	Separation	
Ga – As	$d_1 + (n-1)d_2 + d_3$	
As – As	$2d_3 + (n-1)d_2$	
	$d_1 = 1.90 \text{ \AA}$	$d_2 = 3.15 \text{ \AA}$
		$d_3 = 3.14 \text{ \AA}$

Graphene layers	Ga – As (Å)	As – As (Å)
1	5.04	6.28
2	8.19	9.44
3	11.35	12.59

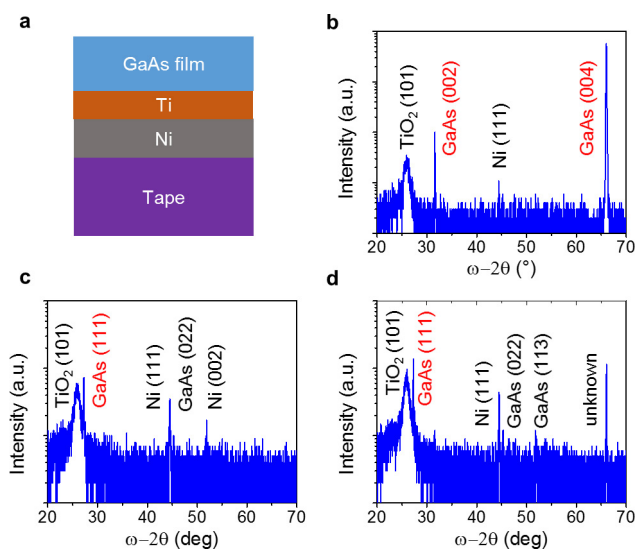
Extended Data Figure 1 | Natural slab separation with n graphene layers present between GaAs slabs. To determine the maximum number of graphene layers that can be inserted within this critical gap, we calculate the natural separation induced by graphene interlayers using the structure shown on the left. The results show that the graphene–As distance d_3 is 3.14 Å, the graphene–graphene distance d_2 is 3.15 Å and the graphene–Ga distance d_1 is 1.9 Å. A detailed description of calculated distances is in the table at the bottom for both Ga–As and As–As terminated cases.



Extended Data Figure 2 | SEM images of front grown surface and released surface of GaAs films grown on monolayer, bilayer and tetralayer graphene stacks transferred onto GaAs(001) substrates.

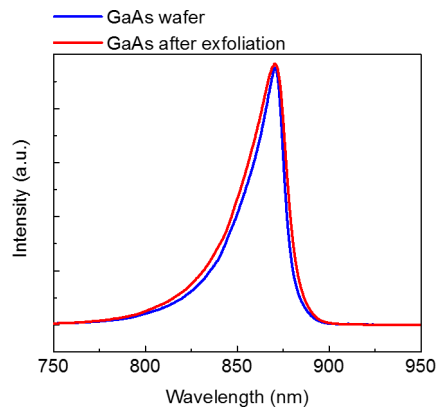
a. The front surface of the GaAs epilayer grown on monolayer graphene–GaAs substrate is generally smooth but also contains impinging marks which need to be addressed by further optimization of nucleation and

growth. Inset, $1\ \mu\text{m} \times 1\ \mu\text{m}$ non-contact AFM scan; the epitaxial layer appears to be growing via step flow growth. The r.m.s. roughness of the AFM scan is 0.3 nm. **b, c.** Three-dimensional growth was observed for films grown on thicker graphene–substrates owing to limited registry from the substrates. Scale bars, $4\ \mu\text{m}$. Top and bottom panels of **a–c** indicate front and released surfaces, respectively.

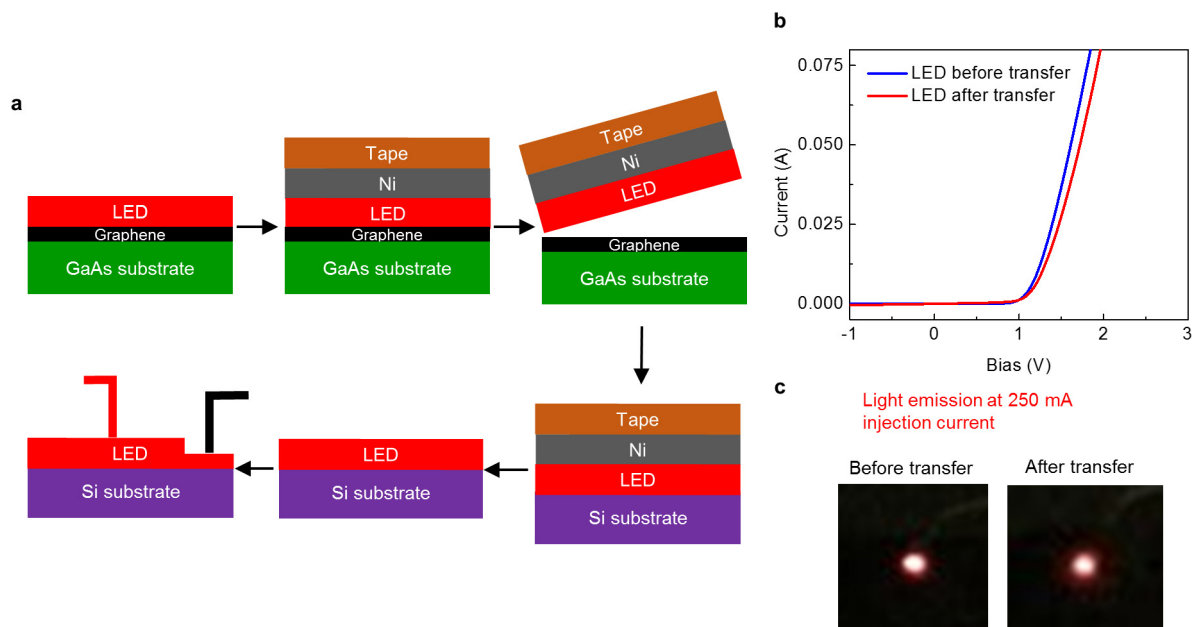


Extended Data Figure 3 | HRXRD ω - 2θ scans of 'exfoliated' GaAs epilayers.

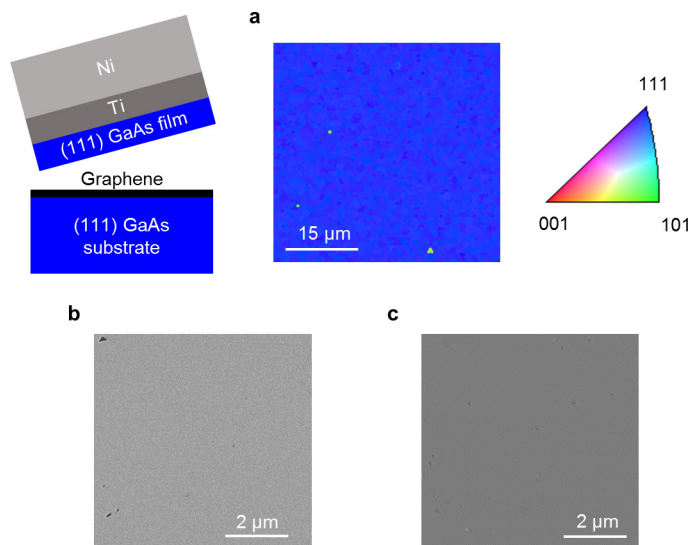
a, Diagram of exfoliated stacks of GaAs released from a graphene-GaAs(001) substrate. **b**, ω - 2θ scan of GaAs exfoliated from monolayer graphene transferred on a GaAs(001) substrate showing (001) single-crystallinity as indicated by XRD peaks of the (002) and (004) lattice labelled in red. **c**, ω - 2θ scan of GaAs exfoliated from bilayer graphene transferred on GaAs(100) substrate showing polycrystallinity with dominant (111) orientation, as indicated by the XRD peak of the (111) lattice labelled in red, and **d**, ω - 2θ scan of GaAs exfoliated from tetralayer graphene transferred on a GaAs(001) substrate showing polycrystallinity with dominant (111) orientation, also indicated by XRD peak of the (111) lattice labelled in red. The ω - 2θ scans also picked up XRD peaks from the Ni stressor film and the Ti adhesion layer that was used to exfoliate the GaAs films (Methods). The presence of these films are shown by the XRD peak of the (111) Ni lattice and the (101) lattice of anatase TiO₂ from the Ti layer.



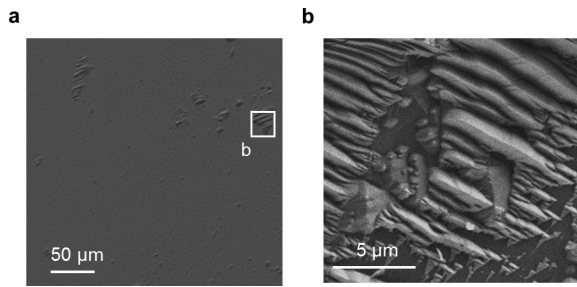
Extended Data Figure 4 | Steady-state room temperature photoluminescence spectra. Shown are steady-state photoluminescence spectra of GaAs substrate and exfoliated GaAs epilayer grown by remote epitaxy.



Extended Data Figure 5 | LED light emission before and after transfer. **a**, Diagram of the graphene-based layer transfer of LEDs. **b**, I - V curves of LEDs before and after transfer. **c**, Light emission of LEDs before and after transfer.



Extended Data Figure 6 | GaAs(111) films grown on a monolayer graphene-GaAs(111)B substrate. Schematic illustration at left shows exfoliation process of a thin-film GaAs(111) epilayer. The EBSD map demonstrates the versatility of the method used to copy the substrate orientation through graphene by remote homoepitaxy. On the right is the inverse pole figure colour triangle for crystallographic orientations. **a**, EBSD map of the released surface of a GaAs(111) layer substrate. **b**, SEM image of the front surface, as grown. **c**, SEM image of the released surface.



Extended Data Figure 7 | Plan-view SEM of exfoliated surface of GaAs.

a, Smooth parts indicate release from graphene, and rough parts indicate spalling directly from GaAs substrate surface through graphene defects. If mechanical defects such as holes and cracks in graphene exist, they permit direct exposure of the GaAs(001) surface to adatoms, resulting in the direct binding of adatoms to the substrate. Location of **b** is shown boxed. **b**, Direct epitaxy of GaAs epilayers on GaAs substrates causes jagged topology (spalling marks) upon exfoliation due to the occurrence of spalling. However, such marks are observed in limited areas.